 doi:10.20944/preprints202105.0608.v1

*Article*

# Green polymer-based nanocomposites containing ceria and their use in the process of stem cell proliferation

**Iosif V. Gofman[1,*], Alexandra L. Nikolaeva[1], Albert K. Khripunov[1], Elena M. Ivan'kova[1], Anton S. Shabunin[2], Alexander V. Yakimansky[1,3], Dmitriy P. Romanov[4], Anton L. Popov[5,6], Artem M. Ermakov[5], Sergey O. Solomevich[7], Pavel M. Bychkovsky[7], Alexander E. Baranchikov[6], Vladimir K. Ivanov[6]**

[1] Institute of Macromolecular Compounds, Russian Academy of Sciences, 199004, Saint Petersburg, Russia; a.l.nikolaeva@imc.macro.ru (A.L.N.); ivelen@mail.ru (E.M.I.); yakimasky@yahoo.com (A.V.Y.)
[2] H.Turner National Medical Research Center for Children's Orthopedics and Trauma Surgery, 196603, Pushkin, Saint-Petersburg, Russia; anton-shab@yandex.ru (A.S.S.)
[3] Saint Petersburg State University, Institute of Chemistry, 198504, Peterhof, Saint-Petersburg, Russia
[4] Institute of Silicate Chemistry, Russian Academy of Sciences, 199034, Saint Petersburg, Russia; dprom@mail.ru (D.P.R.)
[5] Institute of Theoretical and Experimental Biophysics, 142290, Pushchino, Moscow region, Russia; antonpopovleonid@gmail.com (A.L.P.); ao_ermakovy@rambler.ru (A.M.E.)
[6] Kurnakov Institute of General and Inorganic Chemistry, Russian Academy of Sciences, 119991, Moscow, Russia; a.baranchikov@yandex.ru (A.E.B.); van@igic.ras.ru (V.K.I.)
[7] Research Institute for Physical and Chemical Problems of the Belarusian State University, 220030, Minsk, Republic of Belarus; sergeysolomevich@gmail.com (S.O.S.); bychkovsky@tut.by (P.M.B.)
*Correspondence: gofman@imc.macro.ru

**Abstract:** A technique of fabrication of bacterial cellulose-based films with $CeO_2$ nanofiller has been developed. The structural and morphological characteristics of the materials have been studied, their thermal and mechanical properties in dry and swollen states having been determined. The preparation methodology gives way to obtaining composites with the uniform distribution of nanoparticles. The catalytic effect of ceria regarding thermal oxidative destruction of cellulose was confirmed by TGA and DTA methods. An increase in $CeO_2$ content leads to a rise in the elastic modulus (1.27-fold rise caused by the introduction of 5 wt.% of the nanofiller into polymer) and strength of the films. This effect is explained by the formation of additional links between polymer macro-chains *via* the nanoparticles' surface. The materials fabricated are characterized by a limited swellability in water. Swelling causes a 20-30-fold drop in the stiffness of the material, the mechanical properties of the films in a swollen state remaining germane to their practical use. The application of the composite films in cell engineering as substrates for the stem cells proliferation has been studied. The increase in $CeO_2$ content in the films enhanced the proliferative activity of embryonic mouse stem cells. The cells cultured on the scaffold containing 5 wt.% of ceria demonstrated increased cell survival and migration activity. Analysis of gene expression confirmed the improved cultivation conditions on $CeO_2$-containing scaffolds.

**Keywords:** nanocomposites; bacterial cellulose; ceria nanoparticles; thermal properties; swelling; mechanical behavior; biomedical applications; stem cells proliferation; gene expression

## 1. Introduction

In the 21st century, growing attention of researchers and chemical engineers working out novel polymer materials has been drawn to the so-called natural or "green" polymers, including cellulose and its derivatives [1]. Of particular interest are materials based on bacterial cellulose (BC) [2], which is a product of vital activity of *Acetobacteraceae bacteria* (gram-negative anaerobic bacteria) in carbon-containing nutrient media. Typicaly, the media are aqueous solutions of carbohydrates [2], mainly glucose, less commonly saccharose, fructose, maltose, xylose, and polyatomic alcohols, *etc*.

 doi:10.20944/preprints202105.0608.v1



BC is a hydrophilic material with a high degree of structural ordering of macromolecules (the degree of crystallinity is as high as 90-95%). It possesses a complex hierarchical supramolecular structure which consists of ribbon-like fibrils up to 100 nm wide. The fibrils are formed of small nanofibrillar elements with characteristic sizes of 7-10 nm assembled in bundles and tows [1,2].

BC does not contain any contaminants like lignin, pectins, and hemicellulose, present in plant analogues of BC even after purification [2]. BC is characterized by high mechanical strength and stiffness, and the capability of retaining large amounts of water when swelling (up to 98-99% of the total mass of the material depending on preparation technique). Moreover, it is biodegradable and has excellent biocompatibility including one with human tissues. BC has the merits of being non-cytotoxic, non-genotoxic material, causing no allergic reactions of human organism. [3–6].

Great prospects in the development and further modification of "green" materials towards improving their characteristics are associated with the preparation of composites based on BC with either inorganic or organic components [7–10], particularly with nanoparticles. Such an approach is widely used in the fabrication of novel polymer-based materials. Oxide nanoparticles are among the most employed active nanofillers used for the enhancement of polymer properties. The nanoparticles have been proven to alter substantially various properties of materials, such as mechanical, thermal, electrical, and transport ones [11–14]. Therefore, metal oxide nanoparticles are likely to have a profound effect on a number of the cellulose functional properties.

Cerium oxide (ceria) nanoparticles hold promise to be used as an active nanofiller in polymer composites [15]. They were shown to solve the following problems in polymer science: screening of electromagnetic irradiation, fabrication of catalysts, modification of acoustic properties of polymer matrix, *etc* [16–21]. Last but not least, the possibility of using nanosized $CeO_2$ in biomedical nanocomposite materials seems quite promising taking into account a great deal of information on the salient biological activity of ceria. The latter has been reported as an antibacterial [22], antioxidant [23,24] as well as antitumor [25,26] agent. Thus, ceria-containing polymer nanocomposites are anticipated to combine the advantageous properties exhibites by both tha matrix and filler and to reduce their intrinsic drawbacks.

In this paper, we have aimed to thorough investigation of the effect of ceria as active nanofiller on the characteristics of BC-based nanocomposite materials. We have tested their biological activity with a focus to their use in bioengineering, specifically as scaffolds for stem cells proliferation. It has already been shown that bare BC can be used as a substrate facilitating tissue regeneration and possessing cell affinity [27–29]. Therefore, it is reasonable to assess the effect of $CeO_2$ nanoparticles on the cell proliferation on the BC-based scaffolds.

## 2. Materials and Methods

### *Bacterial Cellulose*

BC was produced by *Kommagateibacter xylinus* (acetic acid bacteria, a VKM-880 strain) in aqueous solutions containing 2 wt. % of glucose, 0.3 wt. % of yeast extract and 2 wt. % of ethanol at 30 °C for 14-21 days [30]. The as-prepared BC samples were gel-like pellicles up to 25 mm thick. The pellicles were partially dehydrated by pressing on hand press to fabricate BC films, the BC concentration in the films being about 14 wt. %.

### *$CeO_2$ nanoparticles*

Cerium dioxide nanoparticles with sizes ~3.5-5 nm used in our experiments were synthesized by a modified protocol, reported elsewhere [31]. Briefly, to a water-isopropanol (1:19 vol.) 0.1 M solution of cerium(III) nitrate, a water-isopropanol (1:5 vol.) solution of citric acid (cerium to citrate ratio 1:1) was added to form a white sedi-

 doi:10.20944/preprints202105.0608.v1



ment. The resultant powder was thoroughly washed, dried, and then dispersed in distilled water. To a suspension, concentrated ammonia solution was added, the mixture was refluxed in air at pH 9–10 for 12 h. The resultant ceria sol was boiled for 1 h to remove an excess of ammonia, to pH 8.

*Thin film fabrication*

Pressed BC was fragmented in a high-speed blender (15000 rpm, 15 min) in an aqueous medium (300 ml of water per 1 g of dry BC). The suspension prepared was cast onto a glass support and dried at 160 °C to a constant weight. In order to prepare the nanocomposites, certain amounts of ceria aqueous dispersions (with $CeO_2$ concentration of 1.5%) were poured into the BC aqueous suspension. The films were fabricated using the aforesaid technique. All the films prepared were dense, homogeneous, and ~40 μm thick. The nominal concentrations of $CeO_2$ nanoparticles in the samples were 0 wt. % (bare BC film), 1 wt. %, 3 wt. %, and 5 wt. %.

*Film characterization techniques*

*XRD analysis*

The XRD analysis of the films was performed on a DRON-3M X-ray diffractometer (CuKα - irradiation). The registration of X-ray beam diffraction was carried out according to the Bragg – Brentano scheme [32].

*Scanning electron microscopy*

The surface of the films was studied using SEM. SEM images were obtained with a scanning electron microscope SUPRA-55VP (Carl Zeiss, Germany) using a secondary electron detector as well as a detector of back-scattered electrons. Element maps were collected with an EDX-max 80 $mm^2$ detector (Oxford Instruments, United Kingdom).

*Thermal analysis*

Thermogravimetric (TGA) and differential thermal (DTA) analyses were performed to determine the concentration of remaining water in the films and the exact contents of ceria in the nanocomposite materials. The effect of $CeO_2$ on the kinetics of thermal decomposition of the samples was assessed. A DTG-60 thermal analyzer (Shimadzu, Japan) was used, the samples (~5 mg) being heated in air up to 600 °C with a rate of 5 °C /min.

*Swellability*

To determine the equilibrium water absorption the preliminarily dried at 150 °C samples were weighed and then immersed in the distilled water. The swollen samples were periodically removed from the water, wiped with a tissue, and weighed. The experiment continued until the constant weight had been attained.

The water absorption $W_m$ was calculated with the use of the following equation:

$$W_m = \frac{m_s - m_d}{m_d} \times 100,$$

where $m_s$ and $m_d$ are the weights of the swollen and dry samples, respectively.

*Mechanical properties*

An AG-100kNX Plus setup (Shimadzu, Japan) operating in a uniaxial extension mode was used to study the mechanical characteristics of the films. Strip-like samples (2×30 mm) were stretched at room temperature at a rate of 10 mm/min, according to ASTM D638 requirements. The Young's modulus E, the break stress $\sigma_b$ and the ultimate deformation $\varepsilon_b$ were determined.

 doi:10.20944/preprints202105.0608.v1



*Cell proliferation control techniques*

*Cell culture*

In the experiments, we used mouse mesenchymal stem cells (MSC) at the 3rd passage, harvested from the embryonic skeleton of 13-day-old embryos of the B10GFP/Balb/c hybrid mice carrying a green fluorescent protein (GFP). The cells were received from the vivarium of ICB RAS (Pushchino). The study was conducted according to the guidelines of EU directive 2010/63 of European Parliament and council of Europe Union 09/ 22/ 2010 for the protection of animals used for scientific purposes, and approved by the Institutional Ethics and biosafety committee of Institute of Theoretical and Experimental Biophysics Russian Academy of Sciences. Animal maintenance was in accordance with the rules of Good Laboratory Practice (GLP) and the Order of the Ministry of Health of the Russian Federation No. 199n "Rules of Good Laboratory Practice".

Employing this type of cells was presumed expedient because one needed to avoid applying fluorescent dyes in order to prevent the coloration of the samples under study. Mice were euthanized by cervical dislocation on the 13th day of gestation. Their uteri with embryos were isolated. After the tissue dissociation in the 0.25% trypsin-0.02% EDTA solution (NPO "PanEco", Russia) for 30 min at 37 °C, the cells were collected by centrifugation at 1500 rpm for 2 min. Then, the cells were re-suspended to get a single-cell state in a DMEM/F12 medium (NPO "PanEco", Russia) supplemented with 10% of fetal bovine serum (FBS) (in 1:1 ratio). The resulting suspensions were transferred into vials and cultivated in a 5% $CO_2$ atmosphere at 37 °C in DMEM containing 10% FBS (HyClone), 100 units/ml of penicillin/streptomycin with the addition of 2 mM L-glutamine. When the subconfluent state was reached, the cells were treated with 0.25% trypsin-EDTA solution and seeded into vials in a 1:3 ratio. The cultivation was carried out in a DMEM/F12 medium containing 10% FBS (HyClone), 100 units/ml of penicillin/streptomycin with the addition of 2 mM L-glutamine. Cultures of 2-5 passages were used in the research. The analysis of the viability of cell cultures was carried out using the resazurin assay. After 24-96 hours of cultivation, the cell culture medium was replaced with that one containing 0.02% solution resazurin and the MSC were further cultured.

*Fluorescent microscopy*

The films were cut into 0.8x0.8 cm fragments and placed in the wells of a 24-well plate, under sterile conditions. One sample was assigned to each test point. A sterile cover glass was used as a reference sample. Cells were seeded on the substrates' surfaces. An initial cell seeding density was $30\times10^4$ cells/cm$^2$. The morphological assessment of the cells cultivated on the surfaces of the test materials was implemented on the 1st, 2nd, 3rd, and 4th day of the cultivation in fluorescent light using an inverted microscope Zeiss Axiovert 200.

*Scanning electron microscopy*

The cells were plated on the substrates and cultivated during 24 and 96 hours. The samples were then washed twice for 30 min in phosphate-buffered saline (PBS) with pH 7.4 and dehydrated by passing through alcohols solutions of increasing concentration: 30%, 50%, 70%, 80% for 30 min, and 90% and 100% for 30 min (twice). At the final stage, the samples were placed in a hexamethyldisilazane solution for 24 hours. In order to avoid charge accumulation during scanning the samples were coated with a 2 nm gold layer by ion sputtering in argon atmosphere (0.1 mm Hg). A SUPRA-55VP (Carl Zeiss) microscope was used in the experiments.

*PCR-RT*

Reverse transcription was performed with a Sileks kit (Russia), using an oligo(dT) primer according to the manufacturer's protocol. Produced cDNAs served as a real-time

 doi:10.20944/preprints202105.0608.v1



PCR matrix. For PCR reaction, a mixture was used with SYBR Green dye (Syntol, Russia). To analyze the expression activity of 93 key genes under cell cultivation on the $CeO_2$-containing scaffolds, we used a CFX-96 amplifier (BioRad, USA) or an ABI 7500 Fast Real-Time PCR System (Applied Biosystems, USA). The expression of 96 genes responsible for key cell processes (Supplementary Table S1) was thus determined. Analyzed genes were selected from the database http://www.sabiosciences.com/ for PCR profiling of different biological processes. The level of gene transcription was normalized by the levels of expression of housekeeping genes *β-actin*, *rplp0* (ribosomal protein, large, P0) and *gapdh* (glyceraldehyde-3-phosphate dehydrogenase). The gene-specific primers were selected in the Primer Express program (Applied Biosystems, USA). Each measurement was made twice (internal repetition) and averaged for two independent samples. A sample without reverse transcription stage was used as the control. The obtained expression data were analyzed using online services http://www.sabiosciences.com/, mayday-2.14 software (Center for Bioinformatics, Tübingen, Germany) and Genesis software.

## 3. Results

### *3.1. SEM*

SEM images of the films fabricated (Figure 1) show clearly the structural elements the films are composed of, namely tightly packed fibrils. Comparing the morphologies of the composite and pristine BC films one cannot reveal any noticeable effect of $CeO_2$ nanoparticles on the packing type, except that the BC fibrils in the composite films seem to be aggregated more closely.

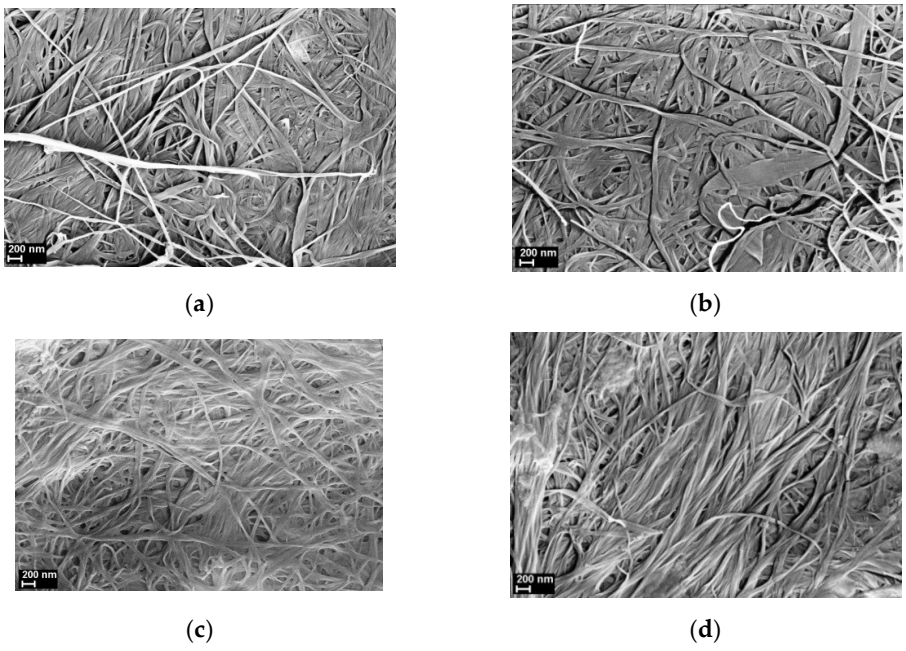


(**a**) (**b**)

(**c**) (**d**)

**Figure 1.** SEM images of the samples studied: (**a**) – bare BC; (**b-d**) – BC-ceria nanocomposite films containing 1 wt. %, 3 wt. %, and 5 wt. % $CeO_2$, respectively.

### *3.2. XRD analysis*

Obviously, the SEM technique does not enable one to distinguish individual filler nanoparticles. Their presence in the films is only evidenced by the comparative analysis of the XRD patterns of the films and pristine $CeO_2$ powder (Figure 2).

Preprints (www.preprints.org) | NOT PEER-REVIEWED | Posted: 25 May 2021 doi:10.20944/preprints202105.0608.v1



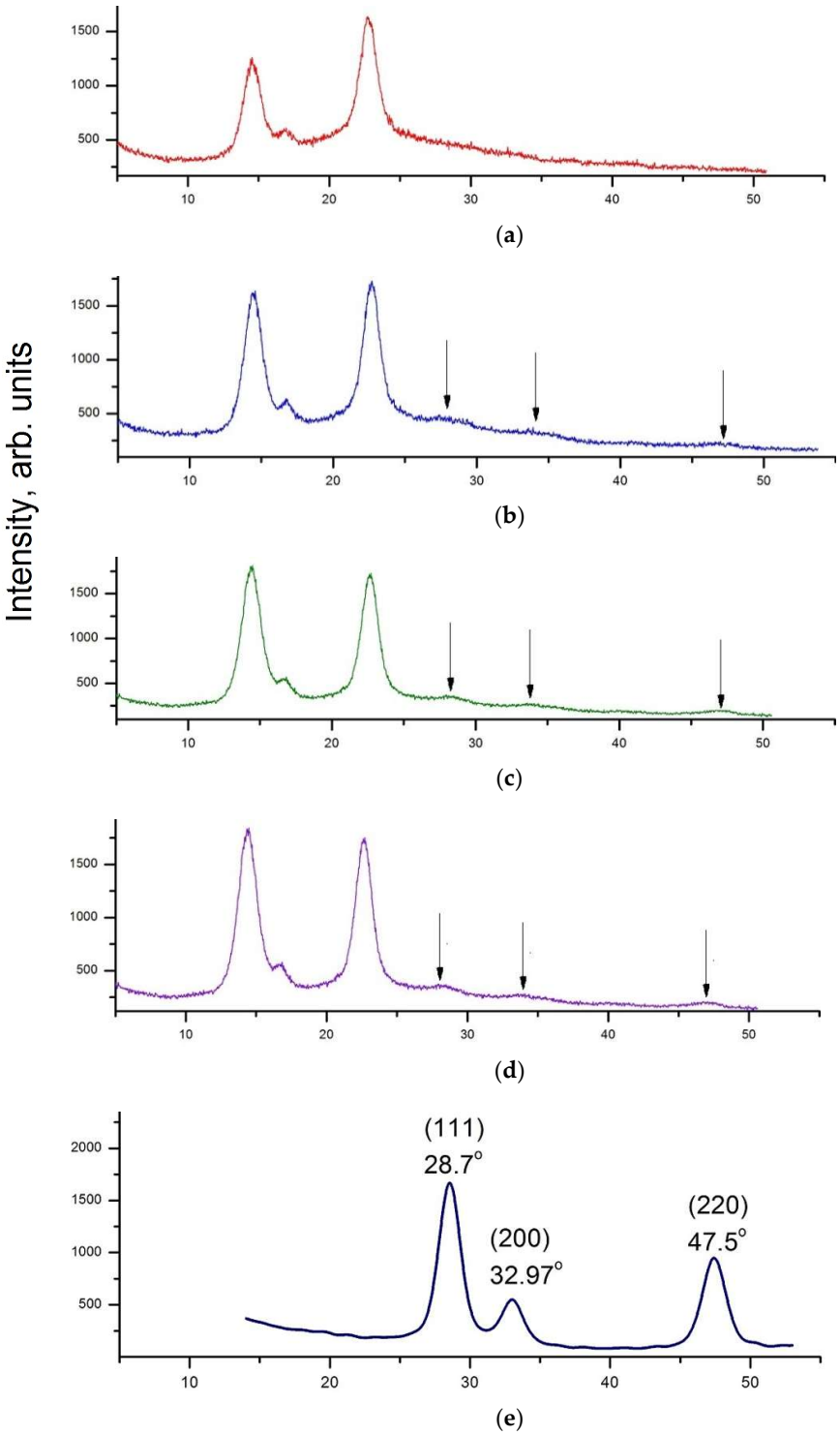


**Figure 2.** XRD patterns of the films: (**a**) bare BC, (**b-d**) BC-ceria nanocomposites with 1 wt. %, 3 wt. % and 5 wt. %, respectively, (**e**) X-ray diffraction pattern of ceria nanoparticles. Arrows in XRD patterns of the composite samples point at $CeO_2$ reflections.

Preprints (www.preprints.org) | NOT PEER-REVIEWED | Posted: 25 May 2021 doi:10.20944/preprints202105.0608.v1



The XRD pattern of $CeO_2$ powder shows sharp reflections at $2\theta$ = 28.7, 32.97, 47.5, and 56.3 deg. attributed to (111), (200), (220), and (311) planes, respectively, and corresponding to the cubic fluorite crystal structure (ICDD PDF card #34-394, data from NIST (National Institute of Standards and Technology, USA)). The full width at half-maximum (FWHM) of the (111) peak was employed in the calculation of the apparent transverse D111 sizes of $CeO_2$ crystals with the use of Scherrer's equation [33]. A $D_{111}$ size was found to be ~5.4 nm. The same reflections along with those of the BC are seen on the patterns of the nanocomposite films (Figure 2b-d). Their intensities increase monotonously with the concentration of ceria nanoparticles in the BC matrix.

*3.3. EDX analysis*

Figure 3 demonstrates the results of energy dispersive X-ray analysis (EDX). This method allows one to map the distribution of elements on the surface of a sample. The results indicate explicitly the presence and increasing concentration of cerium (the areas appearing as speckled yellow in Figure 3c,e) in the samples, images of the latter being given in Figure 3b,d.

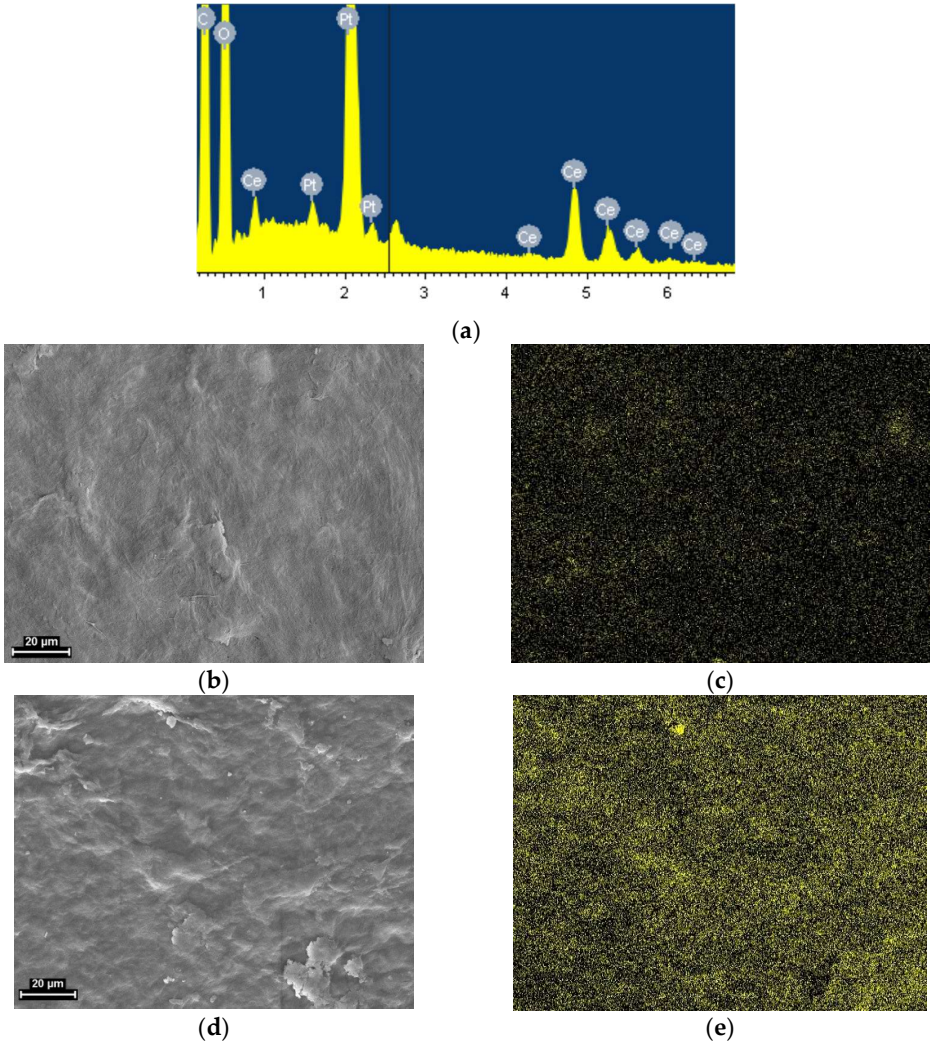


**Figure 3.** (**a**) – An example of EDX spectrum of the composite BC-$CeO_2$ sample; SEM images (left side) and EDX maps of cerium distribution (right side) on the surfaces of the BC-ceria nanocomposite samples with: (**b**, **c**) – 1 wt. % $CeO_2$; (**d**, **e**) – 5 wt. % $CeO_2$.

 doi:10.20944/preprints202105.0608.v1



*3.4. Thermal analysis*

The TGA was used so as to determine precisely the nanofiller concentration in the nanocomposite films prepared (Figure 4). The BC weight loss curve in air (Figure 4a) is attributed to the complete decomposition of the polymer upon heating up to 500 °C accompanied by removal of the gaseous products. A different situation is observed in TGA of the composite films (Figure 4a), *viz.*, after total volatilization of the organic part of the material one can register stable inorganic residues, whose concentrations in the films (1.0 wt.%, 3.05 wt.%, and 4.90 wt.%) correspond to those used in the fabrication of the composite samples.

The TGA curves also enable one to evaluate the weight of water remaining in the as-prepared films. The curves demonstrate an initial weight loss step below 120 °C followed by a plateau at higher temperatures, where the weight does not change up to the beginning of thermal decomposition. The weight loss in all of the samples in this low-temperature region is ~ 2.0-2.5 %. The TGA curves corroborate the literature data [18,34] on the catalytic activity of ceria in decomposition reactions of a number of organic compounds. Comparing the TGA results for the pristine BC film and the composites with various $CeO_2$ contents one can notice that the intense decomposition processes shifts to lower temperatures as ceria concentration increases. Deterioration of thermal stability of the samples is also backed up with a decrease in indices $\tau_5$ and $\tau_{10}$ (the temperature values at which a polymer or a composite loses 5% and 10% of its initial weight, respectively, due to the thermal destruction processes) (Table 1).

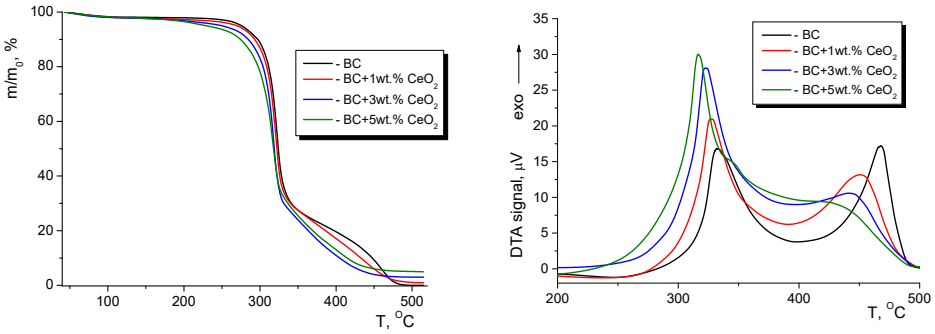


(**a**) (**b**)

**Figure 4.** (**a**) TGA and (**b**) DTA curves of bare BC film and nanocomposite films containing different amounts of ceria.

**Table 1.** Thermal stability indices of the BC and BC-ceria nanocomposite films.

| Sample | $\tau_5$, °C | $\tau_{10}$, °C |
|---|---|---|
| BC | 286 | 302 |
| BC +1 wt.%$CeO_2$ | 283 | 298 |
| BC +3 wt.%$CeO_2$ | 272 | 291 |
| BC + 5 wt.% $CeO_2$ | 261 | 281 |

A detrimental effect of $CeO_2$ on the thermal stability of BC is evident from the DTA curves of the nanocomposite films (Fig. 4b). Indeed, an increase in ceria concentration from 0 to 5 wt.% leads to a gradual shift of exothermic peaks toward the low-temperature region, the peaks being ascribed to the heat effect of thermal destruction. In accordance

 doi:10.20944/preprints202105.0608.v1



with the previously reported data [35,36], the thermooxidative destruction of BC and BC-based nanocomposites occurs in two steps (two peaks on the DTA curves corresponding to these steps are in the 300-330 °C and 420-480 °C temperature regions). The increase in ceria content is seen to result in both a shift of the exothermic peaks to lower temperatures and in a redistribution of the peak heights: a low-temperature peak gets higher whilst the high-temperature one tends to become lower and smoother. In accordance with the well-known scheme of cellulose destruction - Broido-Shafizadeh model [37] - the main reaction taking place in the low-temperature region (up to 350 °C) is the thermally stimulated decomposition of cellulose macrochains resulting in the formation of monomeric and oligomeric fragments (the so-called "sirup" fraction). At the next (high-temperature) stage these fragments decompose further producing a variety of gaseous products. Based on the results obtained in our experiments one could infer that $CeO_2$ causes deep depolymerization of BC and full decomposition of the oligomers into monomers on the first stage of the destruction facilitating the second stage.

It is worth mentioning that all of the aforementioned processes start at temperatures higher than 180-200 °C. One should be mindful of that when thermally sterilizing nanocomposite BC-ceria materials for biomedical applications.

*3.5. Mechanical properties*

The successful practical use of the devised composite materials requires certain mechanical characteristics of the films they form. The mechanical properties of the BC-ceria composite materials with different contents of $CeO_2$ are summed up in Table 2.

**Table 2.** Mechanical characteristics of bare BC and BC-$CeO_2$ composite films.

| Composition | E, GPa | $E_{swollen}/E_{dry}$[1] | $\sigma_b$,MPa | $\varepsilon_b$, % |
|---|---|---|---|---|
| BC | 5.5 ± 0.3 | | 101 ± 5 | 3.6 ± 0.2 |
| BC, swollen | 0.17 ± 0.02 | 0.032 | 4.2 ± 0.4 | 2.9 ± 0.2 |
| BC+1 wt.% $CeO_2$ | 5.8 ± 0.3 | | 96 ± 3 | 2.7 ± 0.2 |
| BC+1 wt.% $CeO_2$, swollen | 0.20 ± 0.02 | 0.034 | 3.6 ± 0.3 | 2.6 ± 0.3 |
| BC+3 wt.% $CeO_2$ | 6.3 ± 0.3 | | 107 ± 3 | 3.3 ± 0.2 |
| BC+3 wt.% $CeO_2$, swollen | 0.24 ± 0.02 | 0.038 | 4.4 ± 0.4 | 2.2 ± 0.1 |
| BC+5 wt.% $CeO_2$ | 6.9 ± 0.4 | | 113 ±5 | 3.3 ± 0.2 |
| BC+5 wt.% $CeO_2$, swollen | 0.30 ± 0.03 | 0.044 | 5.8 ± 0.3 | 2.8 ± 0.2 |

[1] $E_{swollen}/E_{dry}$ is the ratio of the elastic modulus of a film with a given composition in a fully swollen state to that of a dry film

The data given in Table 2 reveal both the high stiffness (Young's moduli of all the materials are higher than 5 GPa) and good strength characteristics (mechanical strength reaches 100-110 MPa) of the films, incorporation of ceria in the BC matrix leading to a gradual (as $CeO_2$ concentration grows) increase in the elastic modulus (5 wt.% of $CeO_2$ augment the modulus by 27%). Such a pronounced rise in the stiffness cannot be attributed to the reinforcing action of the nanofiller upon BC matrix since $CeO_2$ nanoparticles having quasi-spherical shapes (aspect ratio is ~1) and being taken in rather small amounts do not provide the reinforcing effect. A sensible explanation is that additional links between the BC macrochains form *via* the active surface of the nanoparticles when the nanocomposite is fabricated. One should also mention that ceria does not cause a considerable decrease in the ultimate deformation of the films. This confirms the good compatibility between both components of the nanocomposites.

 doi:10.20944/preprints202105.0608.v1



*3.6. Swellability*

The discussion above concerns the mechanical properties of dry films (according to TGA water content is ~2.0-2.5%). However, the capability of a material to absorb water is of crucial importance to a number of practical applications, including biomedicine. Therefore, we studied the impact of ceria upon this property of the BC films.

It is evident from the swelling curves (Figure 5) that the films demonstrate a limited ability to swell in aqueous media, *viz.* the ultimate amount of water in the matrix BC in a swollen state is only 3.25 times higher than the weight of the dry polymer. Apparently, such limited swellability is determined by the characteristics of the intermolecular bonds formed during fabrication of the films.

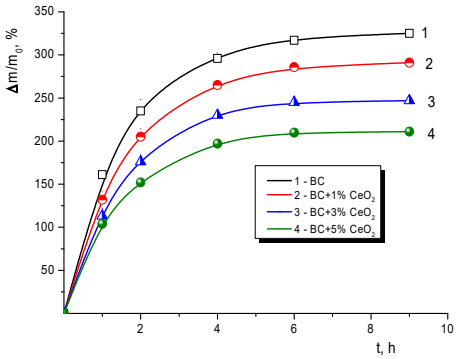


**Figure 5.** Swelling kinetics of bare BC and BC-$CeO_2$ nanocomposite films

A fairly interesting phenomenon observed in the experiments is that the ultimate amount of water in a swollen material drops as $CeO_2$ content increases (Figure 5). This observation corroborates the hypothesis about additional intermolecular interactions, the $CeO_2$ nanoparticles featuring as linkers. A similar effect of reducing the degree of swelling in water was registered in nanocomposite films consisting of a mixture of chitosan with cellulose acetate filled with $CeO_2$ nanoparticles [38].

An assessment of the mechanical properties of the swollen films is necessary when it comes to the practical use of the materials. A technique was developed to perform mechanical tests of the swollen samples. Their mechanical characteristics are given in Table 2. The results show explicitly that even in the extremely swollen state, the films possess a certain mechanical rigidity. The elastic moduli of the samples drop down to 0.03-0.04 of that of a dry film but are of the same order of magnitude as the modulus of LDPE film (170–300 MPa). It should be pointed out that a less pronounced decrease in the elastic modulus caused by swelling was registered in the nanocomposite films in comparison with the pristine BC sample. Such a trend was observed as ceria concentration in the material was augmented: the ratio of the elastic modulus of a film in a fully swollen state to that of a dry film increased from 0.032 to 0.044 when the $CeO_2$ content changed from 0 to 5 wt.% (Table 2). This effect reflects clearly a gradual decrease in swelling degree of the films with a rise in the concentration of the nanoparticles in the BC matrix. Despite a rather significant drop in stiffness, the swollen films are characterized by a mechanical strength of 4-6 MPa, the strength being high enough to use the material in some biomedicine applications.

*3.7. MSC proliferation*

Among the possible applications of BC-ceria nanocomposite materials, their use in bioengineering as scaffolds for the proliferation of stem cells seems to be very promising. One of the main and most auspicious prospects for steady progress in modern medicine

 doi:10.20944/preprints202105.0608.v1



is associated with the development and improvement of the technology for growing the cells of this kind. BC is known to be an interesting and promising material in the manufacture of such substrates [27–29,39]. This is due to the peculiarities of the structure of the material, its excellent biocompatibility combined with the high bioresorption ability, non-cytotoxicity, as well as the possibility of its preparation in an extra-pure state. It seemed appealing to combine such merits of BC matrix with those inherent in ceria in biological systems.

Experiments on the MSC proliferation on the substrates made of bare BC and nanocomposites containing up to 5 wt.% of $CeO_2$ were carried out. Figure 6 shows the data on mouse MSC proliferation activity on the surface of bacterial cellulose, the latter containing various concentrations of $CeO_2$ nanoparticles. The results were registered on the 1st, 2nd, 3rd, and 4th day of cultivation under fluorescent light.

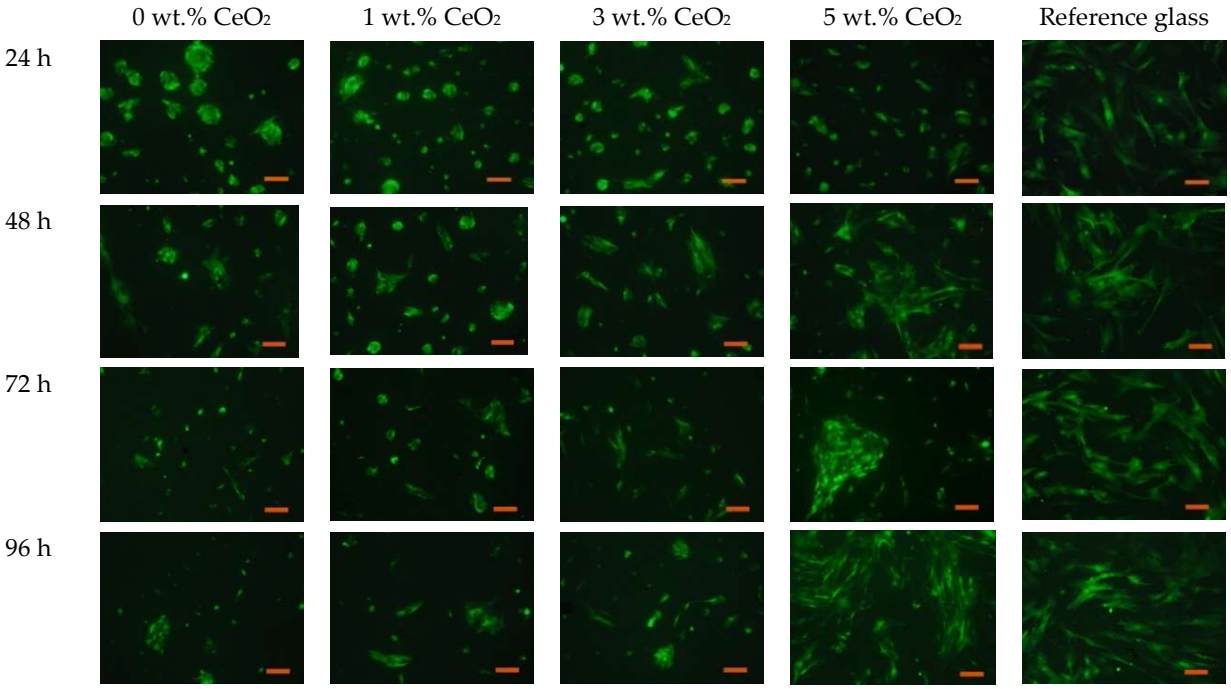


**Figure 6.** Fluorescence microscopy images of mouse MSC with GFP gene on the surfaces of the substrates

The $CeO_2$-containing scaffolds demonstrate good adhesion with the mouse MSC. It is well known that the adhesion of cells to the scaffold surface is strongly affected by the micro-relief and texture of the latter [40]. The addition of $CeO_2$ nanoparticles to the BC matrix is supposed to build up a surface structure most favorable to the formation of focal contacts of the cell filopodia followed by the protrusion of the cell front. A certain electric charge on the scaffold surface also ensures the optimal conditions for proliferation [40]. In the case of BC-$CeO_2$ nanocomposite materials, the electric charge might be provided by the nanoparticles [41].

The adhesive characteristics of the composite scaffolds differ considerably depending on ceria content. The minimum concentration of the nanoparticles (1 wt. %) provided adhesion of a substantial part of the cell culture; however, after 24 hours, morphological features of the cells differed from those on the reference substrate. In particular, the cells did not exhibit the characteristic protrusions and formed multicellular aggregates, whose sizes decreased with an increase in ceria concentration in the scaffold. It might be explained with weak surface micro-relief as well as with the insufficient amount of the initial adhesion sites for the formation of a full-fledged extracellular matrix. Further cultivation on the scaffolds demonstrated that the cells

 doi:10.20944/preprints202105.0608.v1



effectively spreaded on the substrate even at small $CeO_2$ concentrations. This process, though, took more time in comparison with that on the scaffolds with 3 and 5 wt.% of ceria.

It should be pointed out that the scaffolds with high concentrations of $CeO_2$ nanoparticles (3 and 5 wt.%) exhibited notably higher cell viability after 96 hours of cultivation as compared to the scaffolds with 0 and 1 wt.% of the nanoparticles. The quantity of the cells on these scaffolds was also substantially higher than that on the reference sample (cover glass). Thus, one can infer that ceria nanoparticles embedded in a scaffold ensure the increase in the rate of mouse MSC proliferation. This confirms the stimulating action of the hybrid scaffolds against those with no ceria. No difference was registered between the substrates with high $CeO_2$ concentrations and the reference sample at the early stages of cultivation (12, and 24 hours), but longer cultivation periods revealed the well-defined stimulating effect of the former.

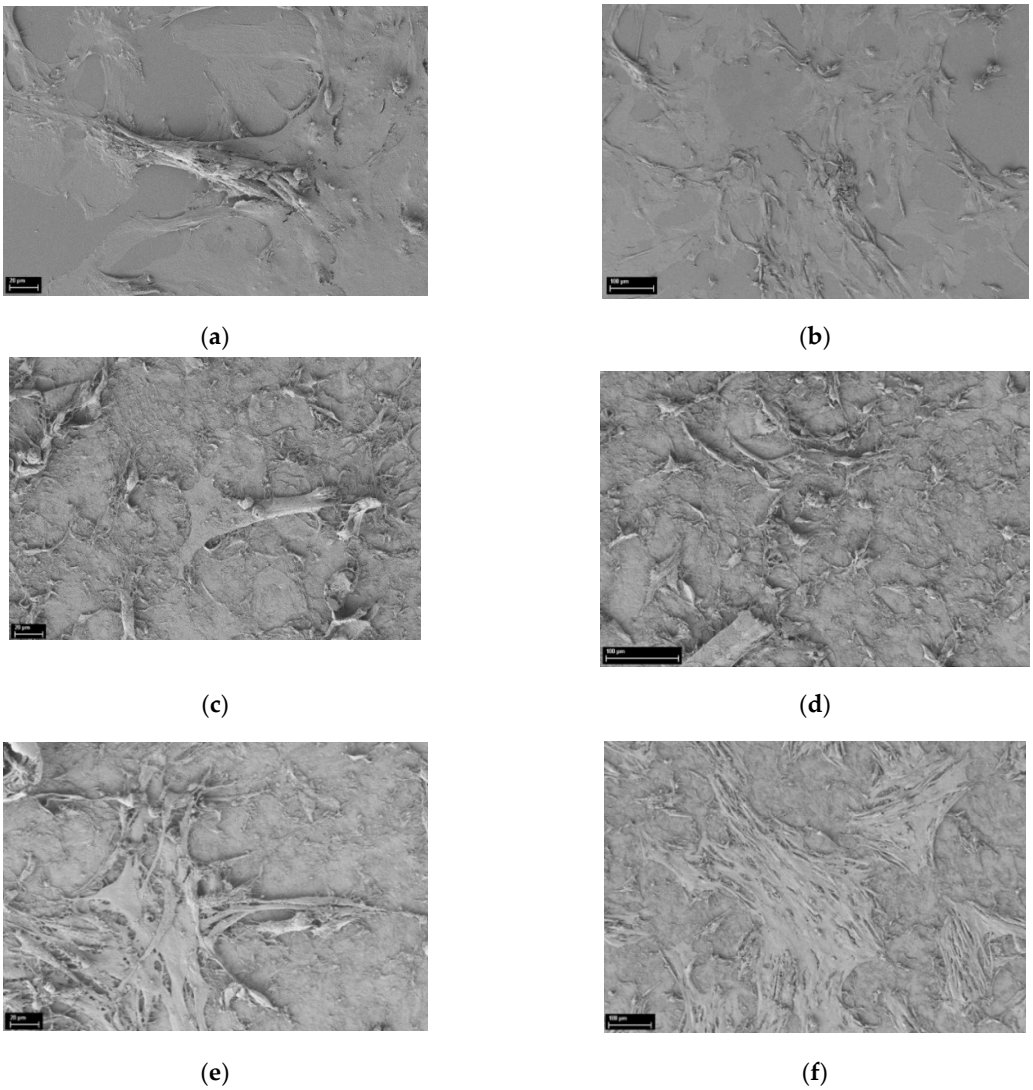

**Figure 7.** SEM images of the scaffolds after 96 hours of mouse mesenchymal stem cells cultivation. a,b – the reference sample (cover glass); c,d – bare BC film; e,f – BC with 5 wt.% of $CeO_2$ nanoparticles

SEM images of the mouse MSC on the surface of BC film with maximal content of $CeO_2$ nanoparticles on the $4^{th}$ day of cultivation are displayed in Figure 7 as compared to those cultivated on bare BC and glass substrate.

 doi:10.20944/preprints202105.0608.v1



Analysis of the SEM images reveals the developed surface microstructure of the scaffolds. Long-term cultivation (96 hours) shows migration and proliferation activity of the mouse MSC on the hybrid $CeO_2$-containing substrates. This is evident from the formation of a bigger portion of the focal contacts as well as from an increase in the protrusion area. The cell monolayer formed on the BC substrates with high $CeO_2$ concentrations (3-5 wt.%) has morphological features typical of actively dividing cells, the features being less pronounced for scaffolds containing 0 and 1 wt.% of ceria.

Quantitative analysis of the number of adhered cells on the $CeO_2$-containing scaffolds showed that all the scaffolds provided effective cell adhesion. The analysis of proliferative activity was carried out during 4 days of cultivation by resazurin test (Figure 8). It was shown that after 48 hours of cultivation, the $CeO_2$-containing scaffolds provide a significant rise in the number of the cells, which is confirmed by increased values of resazurin fluorescence. The results obtained show a dose-dependent effect of ceria-containing substrates on cell culture proliferation.

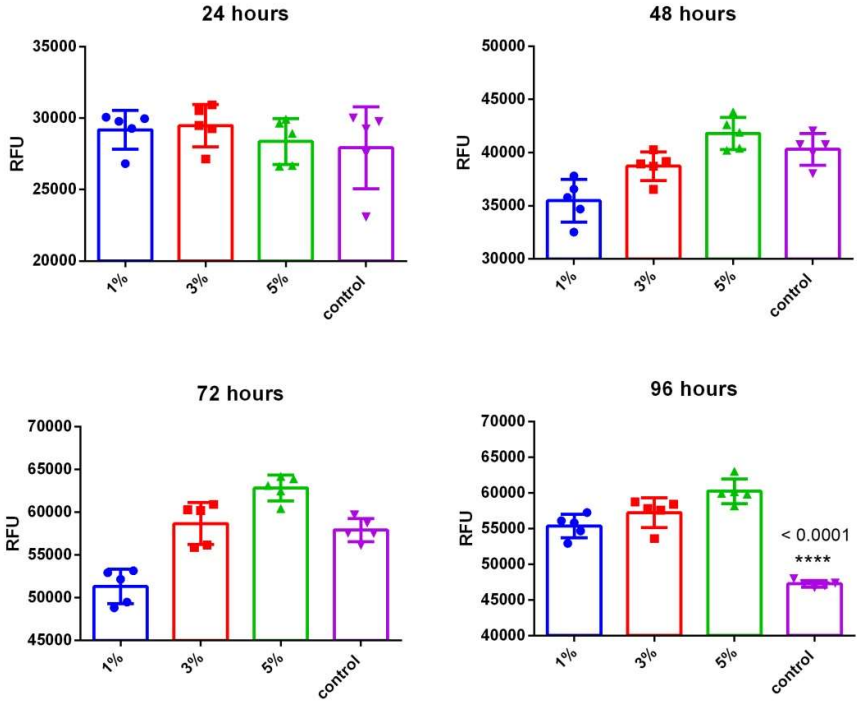


**Figure 8.** Viability of mouse MSC culture after cultivation on $CeO_2$-containing BC scaffolds for 96 hours. Data are presented as mean value ± SD. Cover glass was used as a control. ****-p<0.0001 via

The polymerase chain reaction method (PCR-RT) was used to study the pattern of gene expression (panel of 93 genes) responsible for the activation of a number of cascade pathways, including apoptosis, necrosis, antioxidant system, differentiation, proliferative and migration activities, the repair system and pro-inflammatory response in cells cultured on a substrate containing 0 and 5% $CeO_2$. (Figure 9). After 24 hours, the activation was observed of peroxiredoxin groups, genes PRDX1, NCF1, Nos2, Tro, Noxo1, Noxa1, AOX1, FTH1, Ngb, Nqo1. After 96 hours of cultivation, NCF1, Tro, Noxa1, FTH1, Nqo1 also retained a high level of expression. It should be noted that, according to PCA analysis, ceria-containing substrates demonstrated a significant difference in the gene expression pattern in comparison with ceria-free substrates. The $CeO_2$-containing scaffolds significantly increase the integral index of the upregulation in

Preprints (www.preprints.org) | NOT PEER-REVIEWED | Posted: 25 May 2021 doi:10.20944/preprints202105.0608.v1



the expression pattern of the selected genes, which indicates a pronounced biological activity of these scaffolds.

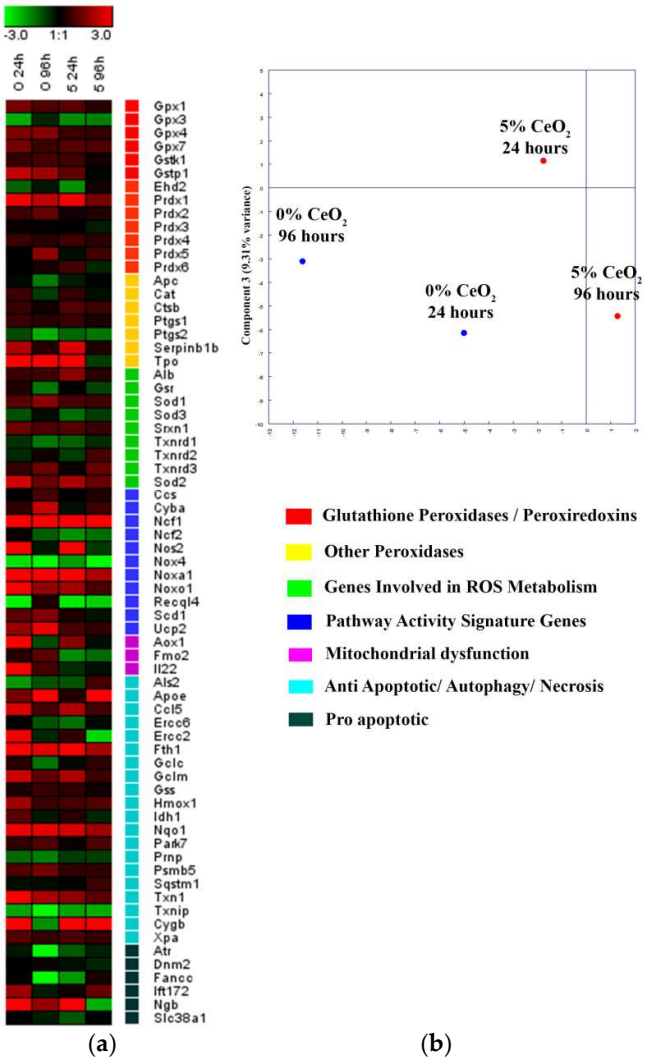


(**a**) (**b**)

**Figure 9.** Heat map of gene expression in mouse MSC cultured on 0% and 5% $CeO_2$-containig scaffolds after 24 and 96 hours of cultivation (**a**). The intensity scale of the standardized expression values ranges from -3 (green: low expression) to +3 (red: high expression, with 1:1 intensity value (black) representing the control (nontreated). Principal component analysis (PCA) of qRT-PCR data for different concentrations of $CeO_2$ scaffold (**b**). Cluster groups of genes and their functionality.

To sum up, one can infer that the MSC proliferation proceeds more effectively on the scaffold with the highest $CeO_2$ concentration used in the work, *i.e.* 5 wt.%. Such a scaffold is characterized by the water absorption value high enough to ensure nutrient exchange capacity sufficient to intense proliferation. We assume that a further increase in the ceria content would facilitate a stimulating activity of the scaffold, its high biodegradability and cytoneutrality being maintained.

 doi:10.20944/preprints202105.0608.v1



## 5. Conclusions

A method of the fabrication of BC-$CeO_2$ composite films was proposed and implemented so as to prepare biologically active materials capable of enduring mechanical stress. A combination of XRD and SEM analyses corroborated a uniform distribution of the nanoparticles in the BC matrix. Simultaneous TGA and DTA revealed a pronounced catalytic activity of ceria regarding the thermooxidative destruction processes in BC-based nanocomposites.

The materials obtained exhibit a limited swellability in an aqueous medium, the addition of ceria to the BC matrix causing a decrease in equilibrium concentration of water in the swollen films. The water content changes from 325 to 210 % of a dry sample's mass upon variation of composition from the bare BC to the film with 5 wt.% of ceria.

$CeO_2$ nanoparticles impart BC films with enhanced stiffness, whose maximum value was observed in the nanocomposite with 5 wt.% of the filler (27% higher than that of the unfilled BC film). Such a rise in stiffness of the material along with a decrease in swellability points at the additional intermolecular interactions *via* the active surfaces of $CeO_2$ nanoparticles. The swollen films have stiffness equaling 0.03-0.04 of that of the dry films, the elastic moduli and strength values being 170-300 MPa and 4-6 MPa. Such characteristics are similar to those of a number of human tissues like muscles, cartilages, and ligaments [42].

It was concluded upon the examination of the nanocomposite materials regarding their use as bioresordable scaffolds for the mouse MSC proliferation that ceria affected positively the cells attachment to a substrate followed by their growth. The ceria-containing scaffolds possess a high adhesion degree with regard to the stem cells *via* the formation of the focal contact of cell filopodia on them. The scaffold with the highest $CeO_2$ concentration (5 wt.%) demonstrated the best cell viability upon 96 hours of cultivation. A cell monolayer formed on this substrate has morphological features typical of an actively dividing culture. The number of cells on the composite substrates was considerably higher than that on a reference sample (glass substrate). Thus, one can infer that the stem cells proliferate faster in the presence of $CeO_2$ nanoparticles. This confirms a stimulating effect of the hybrid substrates compared to the bare BC. The nanocomposite sample with 5 wt.% of ceria is characterized by a water absorption value supposedly high enough to provide good nutrient exchange capacity needed for intensive cell proliferation. BC-based composites containing 5% $CeO_2$ provide upregulation of main clusters of genes responsible for proliferation, migration, metabolism of reactive oxygen species and downregulation of proapoptotic, proinflammatory and mitochondrial dysfunction genes.

**Supplementary Materials:** Table S1: Selected gene groups for PCR-RT analysis.

**Author Contributions:** Conceptualization, I.V.G. and A.L.N.; methodology, I.V.G., A.K.K., E.M.I., S.O.S., A.L.P. and A.E.B.; validation, A.L.N and E.M.I.; formal analysis, A.L.N., I.V.G. and A.V.Y.; investigation, I.V.G., A.L.N., E.M.I., A.S.S., D.P.R., A.L.P. A.M.E., S.O.S. and A.E.B.; resources, A.V.Y., A.L.N., S.O.S., P.M.B. and A.E.B.; writing—original draft preparation, I.V.G. and A.L.N.; writing—review and editing, I.V.G., A.L.N., A.V.Y., A.L.P. and V.K.I.; supervision, P.M.B., A.V.Y. and V.K.I.; project administration, A.V.Y. and V.K.I.; funding acquisition, A.V.Y. and P.M.B.

**Funding:** This research was funded by the Russian Ministry of Education and Science (state contract no. 14.W03.31.0014, MegaGrant). Cell experiments were performed under RFBR grant no. 20-33-70236.

**Acknowledgments:** The authors thank research associates from the Department of Microbiology, St. Petersburg State University, for providing us with bacterial cellulose.

**Conflicts of Interest:** The authors declare no conflict of interest

**References**


1. Rojas, O.J. *Cellulose Chemistry and Properties: Fibers, Nanocelluloses and Advanced Materials*; Rojas, O.J., Ed.; 1st ed.; Springer International Publishing, 2016; Vol. 271; ISBN 978-3-319-79875-2.
2. Esa, F.; Tasirin, S.M.; Rahman, N.A. Overview of Bacterial Cellulose Production and Application. *Agric. Agric. Sci. Procedia* **2014**, *2*, 113-119, doi:10.1016/j.aaspro.2014.11.017.
3. Mitrofanov, R.Y.; Budaeva, V. V.; Sakovich, G. V. Preparation and properties of bacterial cellulose gel films. *Chem. Sustain. Dev.* **2010**, *18*, 503–508.
4. Gromovykh, T.I.; Sadykova, V.S.; Lutcenko, S. V.; Dmitrenok, A.S.; Feldman, N.B.; Danilchuk, T.N.; Kashirin, V. V. Bacterial cellulose synthesized by Gluconacetobacter hansenii for medical applications. *Appl. Biochem. Microbiol.* **2017**, *53*, 60–67, doi:10.1134/S0003683817010094.
5. Bäckdahl, H.; Helenius, G.; Bodin, A.; Nannmark, U.; Johansson, B.R.; Risberg, B.; Gatenholm, P. Mechanical properties of bacterial cellulose and interactions with smooth muscle cells. *Biomaterials* **2006**, *27*, 2141–2149, doi:10.1016/j.biomaterials.2005.10.026.
6. Feng, X.; Ullah, N.; Wang, X.; Sun, X.; Li, C.; Bai, Y.; Chen, L.; Li, Z. Characterization of Bacterial Cellulose by Gluconacetobacter hansenii CGMCC 3917. *J. Food Sci.* **2015**, *80*, E2217–E2227, doi:10.1111/1750-3841.13010.
7. Shah, N.; Ul-Islam, M.; Khattak, W.A.; Park, J.K. Overview of bacterial cellulose composites: A multipurpose advanced material. *Carbohydr. Polym.* **2013**, *98*, 1585–1598, doi:10.1016/j.carbpol.2013.08.018.
8. Nainggolan, H.; Gea, S.; Bilotti, E.; Peijs, T.; Hutagalung, S.D. Mechanical and thermal properties of bacterial-cellulose-fibre-reinforced Mater-Bi® bionanocomposite. *Beilstein J. Nanotechnol.* **2013**, *4*, 325–329, doi:10.3762/bjnano.4.37.
9. Buyanov, A.L.; Gofman, I. V.; Revel'skaya, L.G.; Khripunov, A.K.; Tkachenko, A.A. Anisotropic swelling and mechanical behavior of composite bacterial cellulose-poly(acrylamide or acrylamide-sodium acrylate) hydrogels. *J. Mech. Behav. Biomed. Mater.* **2010**, *3*, 102–111, doi:10.1016/j.jmbbm.2009.06.001.
10. Smyslov, R.Y.; Ezdakova, K. V.; Kopitsa, G.P.; Khripunov, A.K.; Bugrov, A.N.; Tkachenko, A.A.; Angelov, B.; Pipich, V.; Szekely, N.K.; Baranchikov, A.E.; et al. Morphological structure of Gluconacetobacter xylinus cellulose and cellulose-based organic-inorganic composite materials. *J. Phys. Conf. Ser.* **2017**, *848*, 012017, doi:10.1088/1742-6596/848/1/012017.
11. Shah, P. Advancement in Packaging Film Using Microcrystalline Cellulose and $TiO_2$. *Am. J. Polym. Sci. Technol.* **2017**, *3*, 97-102, doi:10.11648/j.ajpst.20170306.11.
12. Bouadjela, S.; Abdoune, F.Z.; Benmoussa, N.; Mechernene, L.; Rahmoun, K.; Maschke, U. Effect of titanium dioxide nanoparticles on polymer network formation. *Spectrosc. Lett.* **2017**, *50*, 522–527, doi:10.1080/00387010.2017.1378683.
13. Tamayo, L.; Azócar, M.; Kogan, M.; Riveros, A.; Páez, M. Copper-polymer nanocomposites: An excellent and cost-effective biocide for use on antibacterial surfaces. *Mater. Sci. Eng. C* **2016**, *69*, 1391–1409, doi:10.1016/j.msec.2016.08.041.
14. Mallakpour, S.; Darvishzadeh, M. Ultrasonic treatment as recent and environmentally friendly route for the synthesis and characterization of polymer nanocomposite having PVA and biosafe BSA-modified ZnO nanoparticles. *Polym. Adv. Technol.* **2018**, *29*, 2174–2183, doi:10.1002/pat.4325.
15. Shcherbakov, A.B.; Reukov, V. V.; Yakimansky, A. V.; Krasnopeeva, E.L.; Ivanova, O.S.; Popov, A.L.; Ivanov, V.K. $CeO_2$ nanoparticle-containing polymers for biomedical applications: A review. *Polymers.* **2021**, *13*, 924, 31 p., doi:10.3390/polym13060924.
16. Lu, Z.; Mao, C.; Meng, M.; Liu, S.; Tian, Y.; Yu, L.; Sun, B.; Li, C.M. Fabrication of $CeO_2$

nanoparticle-modified silk for UV protection and antibacterial applications. *J. Colloid Interface Sci.* **2014**, *435*, 8–14, doi:10.1016/j.jcis.2014.08.015.

17. Liu, K.Q.; Kuang, C.X.; Zhong, M.Q.; Shi, Y.Q.; Chen, F. Synthesis, characterization and UV-shielding property of polystyrene-embedded $CeO_2$ nanoparticles. *Opt. Mater.* **2013**, *35*, 2710–2715, doi:10.1016/j.optmat.2013.08.012.

18. Mullins, D.R. The surface chemistry of cerium oxide. *Surf. Sci. Rep.* **2015**, *70*, 42–85, doi:10.1016/j.surfrep.2014.12.001.

19. Tiefensee, F.; Becker-Willinger, C.; Heppe, G.; Herbeck-Engel, P.; Jakob, A. Nanocomposite cerium oxide polymer matching layers with adjustable acoustic impedance between 4 MRayl and 7 MRayl. *Ultrasonics* **2010**, *50*, 363–366, doi:10.1016/j.ultras.2009.08.012.

20. Jia, R.P.; Wang, C.F.; Zheng, K.S.; He, X.Y.; Huang, M.S. Preparation, characterization, and properties of $CeO_2$/thermoplastic polyurethane nanocomposites. *J. Reinf. Plast. Compos.* **2015**, *34*, 1090–1098, doi:10.1177/0731684415587349.

21. Shang, Z.; Lü, C.; Lü, X.; Gao, L. Studies on syntheses and properties of novel $CeO_2$/polyimide nanocomposite films from Ce(Phen)3 complex. *Polymer.* **2007**, *48*, 4041–4046, doi:10.1016/j.polymer.2007.03.077.

22. Zholobak, N.M.; Ivanov, V.K.; Shcherbakov, A.B. Chapter 12 - Interaction of nanoceria with microorganisms. In *Nanobiomaterials in Antimicrobial Therapy*; William Andrew Publishing, 2016; pp. 419–450, ISBN 978-0-323-42864-4.

23. Zholobak, N.M.; Shcherbakov, A.B.; Vitukova, E.O.; Yegorova, A. V.; Scripinets, Y. V.; Leonenko, I.I.; Baranchikov, A.Y.; Antonovich, V.P.; Ivanov, V.K. Direct monitoring of the interaction between ROS and cerium dioxide nanoparticles in living cells. *RSC Adv.* **2014**, *4*, 51703–51710, doi:10.1039/c4ra08292c.

24. Jiao, X.; Song, H.; Zhao, H.; Bai, W.; Zhang, L.; Lv, Y. Well-redispersed ceria nanoparticles: Promising peroxidase mimetics for $H_2O_2$ and glucose detection. *Anal. Methods* **2012**, *4*, 3261–3267, doi:10.1039/C2AY25511A.

25. Popov, A.L.; Zaichkina, S.I.; Popova, N.R.; Rozanova, O.M.; Romanchenko, S.P.; Ivanova, O.S.; Smirnov, A.A.; Mironova, E. V.; Selezneva, I.I.; Ivanov, V.K. Radioprotective effects of ultra-small citrate-stabilized cerium oxide nanoparticles in vitro and in vivo. *RSC Adv.* **2016**, *6*, 106141–106149, doi:10.1039/c6ra18566e.

26. Shcherbakov, A.B.; Zholobak, N.M.; Spivak, N.Y.; Ivanov, V.K. Advances and prospects of using nanocrystalline ceria in cancer theranostics. *Russ. J. Inorg. Chem.* **2014**, *59*, 1556–1575, doi:10.1134/S003602361413004X.

27. Khan, S.; Ul-Islam, M.; Ullah, M.W.; Ikram, M.; Subhan, F.; Kim, Y.; Jang, J.H.; Yoon, S.; Park, J.K. Engineered regenerated bacterial cellulose scaffolds for application in in vitro tissue regeneration. *RSC Adv.* **2015**, *5*, 84565–84573, doi:10.1039/c5ra16985b.

28. Zhang, C.; Cao, J.; Zhao, S.; Luo, H.; Yang, Z.; Gama, M.; Zhang, Q.; Su, D.; Wan, Y. Biocompatibility evaluation of bacterial cellulose as a scaffold material for tissue-engineered corneal stroma. *Cellulose* **2020**, *27*, 2775–2784, doi:10.1007/s10570-020-02979-0.

29. Zhong, M.; Li, J.; Tang, A.; Zhang, Q.; Ji, D.; Peng, M.; Zhang, R.; Xiong, G.; Wan, Y.; Fan, H. A facile green approach for fabricating bacterial cellulose scaffold with macroporous structure and cell affinity. *J. Bioact. Compat. Polym.* **2019**, *34*, 442–452, doi:10.1177/0883911519877432.

30. Buyanov, A.L.; Revel'skaya, L.G.; Kuznetzov, Y.P.; Shestakova, A.S. Cellulose-poly(acrylamide or acrylic acid) interpenetrating polymer network membranes for the pervaporation of water-ethanol mixtures. *J. Appl. Polym. Sci.* **1998**, *69*, 761–769, doi:10.1002/(SICI)1097-4628(19980725)69:4<761::AID-APP14>3.0.CO;2-S.

31. Ivanova, O.S.; Shekunova, T.O.; Ivanov, V.K.; Shcherbakov, A.B.; Popov, A.L.; Davydova, G.A.; Selezneva, I.I.; Kopitsa, G.P.; Tret'yakov, Y.D. One-stage synthesis of ceria colloid solutions for biomedical use. *Dokl. Chem.* **2011**,

*437*, 103–106, doi:10.1134/S0012500811040070.

32. Kriegner, D.; Matěj, Z.; Kužel, R.; Holý, V. Powder diffraction in Bragg-Brentano geometry with straight linear detectors. *J. Appl. Crystallogr.* **2015**, *48*, 613–618, doi:10.1107/S1600576715003465.

33. Calleja, E.; Balta; Vonk, C.G. X-ray Scattering of Synthetic Polymers (Polymer Science Library 8). *Elsevier* **1989**, 317.

34. Carltonbird, M.; Eaimsumang, S.; Pongstabodee, S.; Boonyuen, S.; Smith, S.M.; Luengnaruemitchai, A. Effect of the exposed ceria morphology on the catalytic activity of gold/ceria catalysts for the preferential oxidation of carbon monoxide. *Chem. Eng. J.* **2018**, *344*, 545–555, doi:10.1016/j.cej.2018.03.111.

35. Gao, M.; Wu, W.H.; Wu, F.C. Thermal degradation and smoke suspension of cotton cellulose modified with THPC and its lanthanide metal complexes. *J. Therm. Anal. Calorim.* **2009**, *98*, 245–251, doi:10.1007/s10973-009-0122-4.

36. Silva, M.C.; Lopes, O.R.; Colodette, J.L.; Porto, A.O.; Rieumont, J.; Chaussy, D.; Belgacem, M.N.; Silva, G.G. Characterization of three non-product materials from a bleached eucalyptus kraft pulp mill, in view of valorising them as a source of cellulose fibres. *Ind. Crops Prod.* **2008**, *27*, 288–295, doi:10.1016/j.indcrop.2007.11.005.

37. Bradbury, A.G.W.; Sakai, Y.; Shafizadeh, F. A kinetic model for pyrolysis of cellulose. *J. Appl. Polym. Sci.* **1979**, *23*, 3271–3280, doi:https://doi.org/10.1002/app.1979.070231112.

38. Kalaycıoğlu, Z.; Kahya, N.; Adımcılar, V.; Kaygusuz, H.; Torlak, E.; Akın-Evingür, G.; Erim, F.B. Antibacterial nano cerium oxide/chitosan/cellulose acetate composite films as potential wound dressing. *Eur. Polym. J.* **2020**, *133*, 109777, 7 p., doi:10.1016/j.eurpolymj.2020.109777.

39. Svensson, A.; Nicklasson, E.; Harrah, T.; Panilaitis, B.; Kaplan, D.L.; Brittberg, M.; Gatenholm, P. Bacterial cellulose as a potential scaffold for tissue engineering of cartilage. *Biomaterials* **2005**, *26*, 419–431, doi:10.1016/j.biomaterials.2004.02.049.

40. Vesel, A.; Junkar, I.; Cvelbar, U.; Kovac, J.; Mozetic, M. Surface modification of polyester by oxygen- And nitrogen-plasma treatment. *Surf. Interface Anal.* **2008**, *40*, 1444–1453, doi:10.1002/sia.2923.

41. Asati, A.; Santra, S.; Kaittanis, C.; Perez, J.M. Surface-charge-dependent cell localization and cytotoxicity of cerium oxide nanoparticles. *ACS Nano* **2010**, *4*, 5321–5331, doi:10.1021/nn100816s.

42. Chang, H.-I.; Wang, Y. Cell Responses to Surface and Architecture of Tissue Engineering Scaffolds. In *Regenerative Medicine and Tissue Engineering - Cells and Biomaterials.* Eberli, D. Ed.; InteshOpen, **2011**, doi:10.5772/21983.